





# An optimized design modelling of PV integrated SEPIC-based four-switch inverter for sensorless PMLDC motor control

Poovizhi Mani, Senthil Kumaran Mahadevan, Anitha Roseline Johnson and Murugesan Kullan

Department of EEE, Sri Sivasubramaniya Nadar College of Engineering, Kalavakkam, India

## ABSTRACT

The design of PV-based high gain SEPIC converter integrated with four-switch strategy, which has been used to achieve sensorless speed control of Permanent magnet Brushless DC motor (PMLDC) is analysed in this work. Hence SEPIC converter coupled with Fuzzy Logic, MPPT Algorithm is employed to retain voltage. SEPIC converter is chosen as it has a continuous current operation with high gain; Fuzzy MPPT algorithm is used as it provides accurate results faster while the classical MPPT techniques provide the results with fluctuations in attaining the maximum power. Regarding the sensorless control of PMLDC motor, the conventional six-switch strategy is replaced by four-switch strategy and the sensors are replaced by back EMF method. Four-switch strategy has the capability of reducing the losses, size, cost and complexity of control. For achieving the nominal speed, a closed-loop control is implemented with PI controller, which is tuned by GWO technique. The proposed methodology is more efficient as the motor speed remains unchanged even under the full load condition. The end result of traditional PI algorithm and PI algorithm, which have been tuned by GWO algorithm, is compared and simulated through MATLAB. This is also implemented and validated in hardware by FPGA Spartan 6E controller.

## ARTICLE HISTORY

Received 22 July 2021  
Accepted 12 November 2021

## KEYWORDS

BLDC motor; SEPIC converter; four-switch VSI; PI controller; speed control; GWO algorithm; Fuzzy Logic MPPT algorithm

## 1. Introduction

Brushless DC motor is commonly utilized in a wide range of applications as it has higher efficiency, higher power factor, higher torque, low maintenance and ease of control, along with these advantages, this motor has high accessibility in various power ratings. Initially, DC and AC motors are used and their usage has been limited as its efficiency and losses have affected the working process of the entire system [1]. To overcome this issue, BLDC motor has been preferred. The speed control of the BLDC motor is achieved through conventional PI controllers, the performance of which is affected by the load disturbances and speed variations. Hence the behaviour of BLDC motors is enhanced by the digital control schemes [2–5]. An improved switching strategy for BLDC fan drive is discussed in [6], which increases the energy alteration efficiency of the system. In [3], a single dead beat controller is employed to control the three-phase current, which results in zero steady-state error. In [7], the functionality of the BLDC motor drive is improved by microcontrollers, which are tuned through the external optimization algorithm instead of sensors. A reliable operation of BLDC motor in low-speed range and a modification, which is done to find the exact commutation points in high-speed range, have been discussed in [8]. In [9], the optimal

commutation control is achieved and the feasibility of linearization is analysed. The  $3\phi$  inverters are utilized for driving the motors with conventional six switch topology. These inverters are subjected to only low power applications; the current and voltage ratings of the switches are to be enhanced for high power applications. But by increasing the rating of the switches, it is possible to enhance the performance of the six-switch topology [10].

The precise control of the motor is guaranteed only if the rotor position is known and hall sensors are utilized for sensing the rotor position which are expensive. Now a days, sensorless speed control has attracted many researchers and some of the articles which employs sensorless approach are reviewed as follows: a high-frequency sensorless control of five-phase BLDC in the frequency domain is established in [11]. As the hall-effect sensors are highly sensitive in temperature, the control of the BLDC motor is unreliable, which can be overcome by sensorless control of BLDC motors [12]. A simple and cost-effective control technique, which excludes the DC–DC conversion stage for a PV-fed BLDC motor water pump is discussed in [13]. A position sensorless BLDC driven solar water pump is validated, which has the advantages of eliminating virtual neutral potential, simple structure and low cost [14].

For the PV system, the bidirectional energy controller is used, which operates for 24 hours without any change in weather with enhanced reliability [15].

Generally, the outcome of PV is low voltage DC and to boost the voltage, DC-DC converters are utilized. Some of the commonly used converters are boost, buck-boost, CUK. The voltage-gain ratio of these converters is low [16–18]. Depending on the weather, the PV output varies. The necessity of MPPT algorithms is essential to extricate the maximum power from PV. Classical MPPT algorithms such as P&O, incremental conductance and so on are easy to implement but show more fluctuations around MPP whereas the intelligent-based MPPT algorithms such as Fuzzy, ANN and so on provide accurate results at a high speed [19, 20].

In this paper, sensorless speed control in PV fed BLDC motor is proposed, in which the conventional six-switch VSI is replaced by four-switch VSI incorporated with direct back EMF method, which results in the reduction of losses, size and cost. Adding to that, the maximum power of the PV system is extracted by Fuzzy

Logic Algorithm-based SEPIC converter. The effective speed control of the BLDC motor is accomplished by using GWO-PI controller, which provides better settling time when analogized with the PI controller.

The schematic representation of the proposed method is depicted in Figure 1. The mathematical formulation for the PV system, SEPIC converter, Fuzzy MPPT algorithm, Four-switch VSI, Sensorless control, BLDC motor and GWO algorithm is elaborated in the upcoming sections.

## 2. Proposed control methodology

The control scheme (Figure 2) starts with the solar array. The outcome of the solar array is linked to the SEPIC converter, which is highly fluctuated since it mainly depends on the weather conditions. When an input of 60 V is given to a single-ended primary inductor converter, an output voltage of 300 V is attained. The gain in SEPIC converter is 1:8, it only boosts the voltage and it is not possible to maintain the voltage as constant.

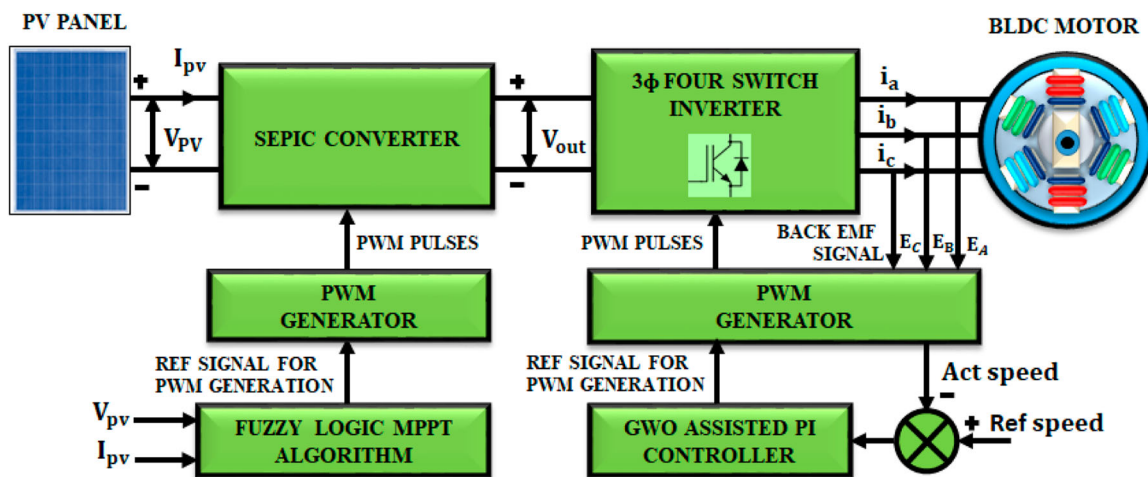


Figure 1. Proposed speed control of four-switch VSI based BLDC motor without sensor.

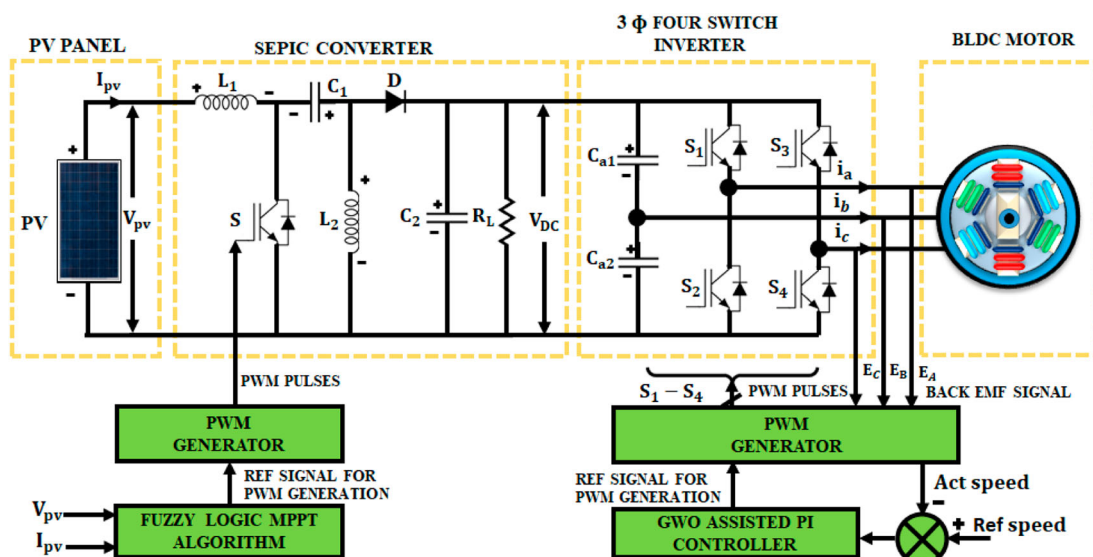


Figure 2. Proposed control circuit.

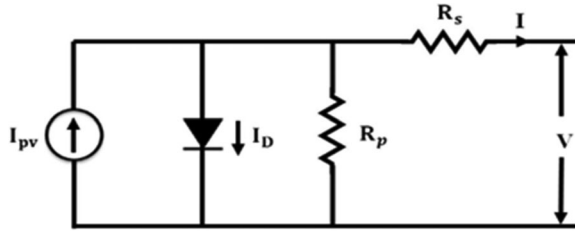


Figure 3. Representation of a PV system.

Hence, Fuzzy Logic MPPT Algorithm is proposed to maintain the voltage almost as constant (Figure 3).

The actual values are taken by giving a delay of 10 ms and the errors are calculated, which is given as input to the Fuzzy Logic MPPT Algorithm. The first step is pre-processing, by which the noises are removed. The second step is Fuzzification, in which Mamdani-based triangular membership function is used. The third step is the rule-based inference engine, in which 49 rules are framed. The fourth step is Defuzzification in which the error is normalized and finally the obtained signal is given to the PWM generator. The pulses generated by the PWM generator are given to the SEPIC converter by which the output of the SEPIC converter is maintained without oscillations.

When the load is applied, the speed in the motor reduces. The reference signal is generated by a PI controller tuned using Grey Wolf Optimization and is given to the PWM generator. Here, the reference signal is compared using carrier signal and the pulses are given to the inverter and then it is observed that the motor has been run efficiently even under the full load condition. In real time, FPGA Spartan 6E controller can be implemented in hardware.

### 3. Modelling of proposed scheme

#### 3.1. Input PV panel

Generally, a PV module's operating point varies with respect to the changes in temperature and irradiance. The schematic representation of the PV array is shown as follows.

The fundamental current ( $I$ ) equation of a PV system is as follows:

$$I = I_{pvcell} - I_{ocell} \left[ \exp \left( \frac{qv}{akT} \right) - 1 \right] \quad (1)$$

$$I = I_{pv} - I_o \left[ \exp \left( \frac{(v + R_s I)q}{aV_k} \right) - 1 \right] - \frac{(v + R_s I)}{R_p} \quad (2)$$

where  $I_{pv}$  is the photovoltaic current,  $I_o$  is the overloaded current,  $V_k \rightarrow \frac{kT}{q}$ ,  $q$  indicates the charge of the electron,  $a$  is the ideality factor,  $v$  is the voltage over the diode,  $k$  is the Boltzmann constant,  $T$  is the temperature coefficient,  $R_p$  is the parallel resistance of PV,  $R_s$  is the series resistance. As the temperature and irradiation

have varied, the stored power in the PV also gets varied and so Equation (2) becomes

$$I = I_{pv} - I_o \left[ \exp \left( \frac{(v + R_s I)q}{akT.N_s} \right) - 1 \right] - \frac{(v + R_s I)}{R_p} \quad (3)$$

where  $N_s$  is the number of series in PV array.

#### 3.2. Single ended primary inductor converter (SEPIC)

This is generally a DC–DC converter either increases or decreases the output potential by varying the duty cycle ratio of the switch  $S$ . One unique feature of SEPIC is that the polarity of the output is same as that of input. Generally, SEPIC converters are operated in a continuous conduction state and the current through  $L_1$  never drops to null value. The schematic illustration of SEPIC is as shown in Figure 4.

Under steady-state operating conditions, the potential on capacitor  $C_1$  is as same as the supply potential  $V_{PV}$ . Because of this reason, the average current through  $L_2$  is identical with the to the  $V_{PV}$  independent average load current. The average voltage equation is mentioned as follows:

$$V_{PV} = V_{L_1} + V_{C_1} + V_{L_2}$$

As the average voltage of the capacitor ( $V_{C_1}$ ) and the input voltage ( $V_{PV}$ ) are same, the above equation can be rewritten as

$$V_{L_1} = -V_{L_2} \quad (4)$$

The mutual inductance values  $L_1$  and  $L_2$  have been zero, as their voltages are equal in magnitude. Therefore, the ripple current of the inductors also has the same magnitude. Hence the average current has been mentioned through the subsequent equation:

$$I_D = I_{L_1} - I_{L_2} \quad (5)$$

#### Mode 1 operation

The circuit in Figure 5 illustrates the working condition of SEPIC converter when the switch  $S$  is ON. In this mode of operation, the current through  $L_1$  and  $L_2$  has been increased with opposite polarity.  $L_1$  gets the power through the input source. Since switch  $S$  is closed, the voltage over the  $C_1$  is approximately same as

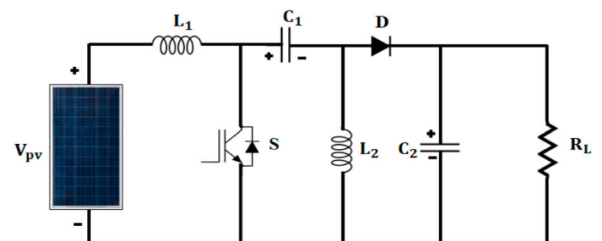


Figure 4. SEPIC converter.

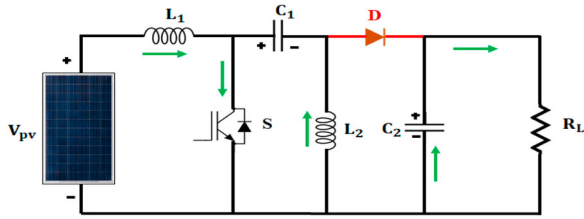


Figure 5. Mode 1 – SEPIC converter.

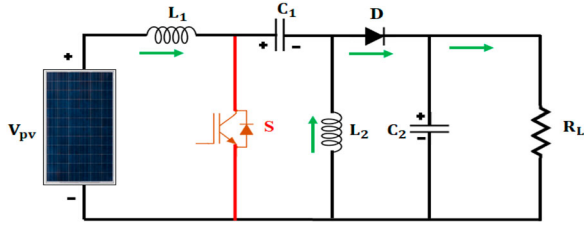


Figure 6. Mode 2 – SEPIC converter.

$V_{PV}$  and potential across  $L_2$  is approximately equal to  $-V_{PV}$ . Thus the energy, which is supplied by  $C_1$  helps in increasing the amplitude of the current through  $L_2$  and so the power, which is gathered in the  $L_2$  gets increased.

### Mode 2 operation

The circuit in Figure 6 shows the working process of the SEPIC converter when the switch  $S$  is OFF. In this mode of operation, the current through  $C_1$  and  $L_1$  becomes the same and the current through  $L_2$  continues in the negative direction as in mode 1 operation. It is observed from the circuit that the current from  $L_1$  and  $L_2$  is added to increase the current, which is distributed to the load. By applying Kirchhoff's Current law,

$$I_D = I_{C_1} - I_{L_2} \quad (6)$$

It is also noted that  $C_1$  is charged by  $L_1$  during the second mode of operation and gets recharged through  $L_2$  during the first mode of operation.

The following are the formulas used for calculating the parameters:

$$\text{Duty cycle, } D = \frac{V_{OUT} + V_D}{V_{IN} + V_{OUT} + V_D} \quad (7)$$

Ripple current in  $L_1$  and  $L_2$ ,

$$\Delta I_L = I_{IN} \times 40\% = I_{OUT} \times \frac{V_{OUT}}{V_{IN(\min)}} \times 40\% \quad (8)$$

$L_1$  and  $L_2$  are given as

$$L_1 = L_2 = L = \frac{V_{IN(\min)}}{\Delta I_L \times f_{sw}} \times D_{\max} \quad (9)$$

The SEPIC converter's output has only boosted the value of the voltage and for maintaining the voltage, certain algorithms are needed.

Table 1. Table of rules.

ERROR ( $e$ )	NB	NB	NS	PS	PM	PB
	NB	NB	NS	PS	PM	PB
	NM	NB	NS	NM	NS	ZE
	NS	NB	NB	NM	NS	PS
CHANGE IN ERROR ( $ce$ )	ZE	ZB	NM	NS	PS	PM
	PS	NM	NS	ZE	PS	PM
	PM	NS	ZE	PS	PM	PB
	PB	ZE	PS	PM	PB	PB

### 3.2. Fuzzy logic maximum power point tracking method

To get the extreme power from solar module irrespective of climatic variations, certain MPPT techniques are implemented. In the literature, the outcomes of multiple algorithms are discussed, among that the P&O technique is simple but it exhibits disadvantages like slow convergence and oscillations in the output. Hence an effective Fuzzy MPPT algorithm is proposed to get the desired output. The desired PWM pulse is generated by means of the Fuzzy algorithm and it is given to the SEPIC converter to retain the voltage. By giving a delay of 10ms, the actual values are computed and thus the error is computed. Here, error ( $e$ ) and change in error ( $ce$ ) are set to the input of Fuzzy controller, which can be evaluated as

$$e(k) = \frac{P_{PV}(k) - P_{PV}(k-1)}{V_{PV}(k) - V_{PV}(k-1)} \quad (10)$$

$$ce = e(k) - e(k-1) \quad (11)$$

where  $V_{PV}$ ,  $P_{PV}$  are voltage then power at PV individually and the number of iterations is denoted by  $k$ .

The input  $e(k)$  is taken as the curve slope by which the location at which the maximum power obtained can be decided and  $ce$  describes the movement of the operating point in which the MPP moves. MPPT curve of control is depicted in Figure 7(a).

During Fuzzification, an input signal is processed and fuzzy values are assigned to them by seven fuzzy subsets. Here, Mamdani-based triangular membership function is used. In the inference engine, data interpretation is carried out by considering 49 rules (Table 1) and their membership functions. In the centroid-based defuzzification segment, the fuzzy information is converted into normalized data. Depending on the location of the operating point, the output can be obtained through the change in duty cycle ( $\Delta D$ ). The flow chart of Fuzzy MPPT is shown in Figure 7(b).

By using the Fuzzy algorithm, the duty cycle for controlling the switch of SEPIC converter is obtained. Whenever the PV voltage is high, the duty cycle is low and whenever the PV voltage is low, the duty cycle is more. Hence the rules are framed based on this logic.

Based on the above table, the fuzzy rules are framed as follows:

Rule 1: If  $e$  is NB and  $ce$  is NB, then  $\Delta D$  is NB

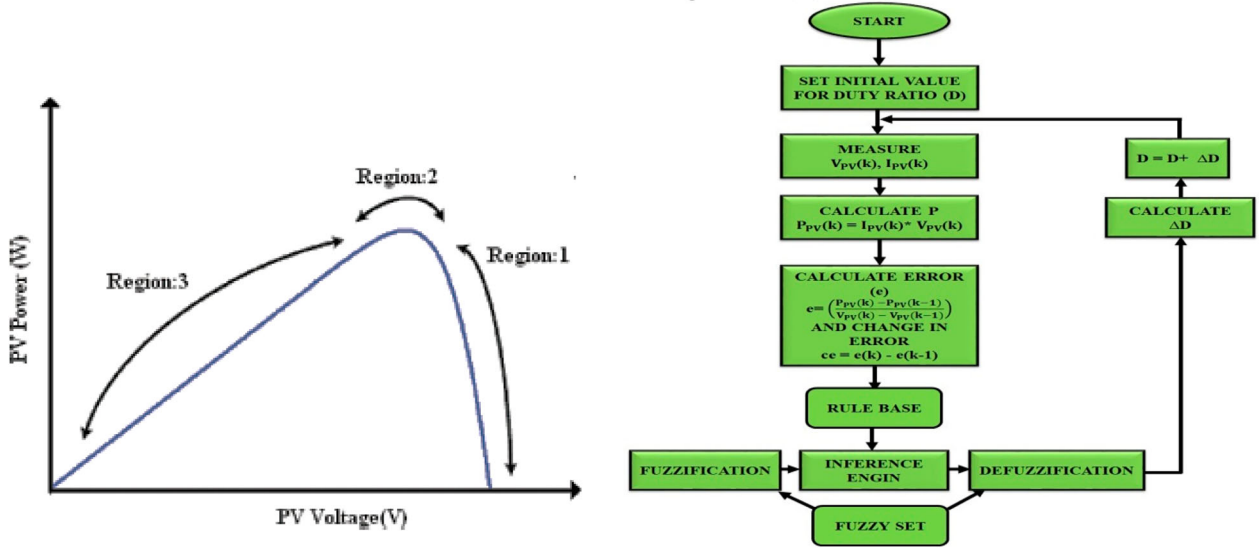


Figure 7. (a) MPPT curve of control and (b) flowchart for Fuzzy MPPT algorithm.

Rule 2: If  $e$  is NM and  $ce$  is NB, then  $\Delta D$  is NB

...

Rule 49: If  $e$  is PB and  $ce$  is PB, then  $\Delta D$  is PB

The error value is the difference of the PV voltage obtained at the present time and the previous time. If the error is negative minimum and the change in error is positive big, which implies that the duty cycle is less. The minimum value of the duty cycle is taken as 0.55 and the maximum value of the duty cycle is taken as 0.8.

By using the Fuzzy MPPT algorithm, desired pulses are obtained as output from the PWM generator and then fed into the SEPIC converter. By this, the SEPIC converter's output is retained irrespective of the changing weather. Now the converter output is fed to the four-switch VSI.

### 3.3. Four-switch VSI

Generally, six-switch VSI is used as the control circuit for Brushless DC motors to achieve speed control in which the losses, cost and size are more. Here, the two switches are replaced by two capacitors. In the operation of four-switch VSI, it is noted that the switches of the same leg cannot be switched on at the same time. The phase that is linked to the middle of the capacitor is uncontrolled and hence in each operating mode, one phase has been remained inactive (silent) and the other two phases are in conducting mode (active). The switching strategy of four-switch VSI is shown in Table 2 and the schematic representation is as in Figure 8.

### 3.4. Sensorless speed control of brushless DC motor

In this paper, a sensorless approach is implemented and carried out using back EMF detection scheme, through

Table 2. Switching strategy of four-switch VSI.

Modes	Switching devices	Active phases	Silent phases
Mode 1	$S_4$	B,C	A
Mode 2	$S_1, S_4$	A,B	C
Mode 3	$S_1$	A,C	B
Mode 4	$S_3$	B,C	A
Mode 5	$S_2, S_3$	A,B	C
Mode 6	$S_2$	A,C	B

which the implementation cost and system size are reduced to a great extent. BLDC motor generates back EMF, which is fed to the PWM generator, through that the required signal is generated to run the motor.

BLDC motor's speed has been regulated either with sensor or without sensor. However, for lessening the assembly cost, sensorless control can be preferred in the place of sensors. When these sensors are not capable to work in some tough environments, sensorless control is highly preferred. This can be achieved by back EMF detection scheme. This detection is based on zero-crossing estimates of the EMF waveform, which is done by knowing the terminal voltage.

The terminal voltages of four-switch equations  $V_{an}$ ,  $V_{bn}$ ,  $V_{cn}$  are as follows:

$$V_{an} = R_a i_a + L_a \frac{di_a}{dt} + E_A \quad (12)$$

where  $R_a$  denotes the stator resistance,  $L_a$  denotes the phase inductance,  $E_A$  and  $i_a$  are the back EMF and the phase current at phase A. Likewise for the other two phases, the voltage equation can be as follows:

$$V_{bn} = R_b i_b + L_b \frac{di_b}{dt} + E_B \quad (13)$$

$$V_{cn} = R_c i_c + L_c \frac{di_c}{dt} + E_C \quad (14)$$

The line equation for line voltage can be mentioned as follows:

$$V_{ab} = R(i_a - i_b) + L \frac{d(i_a - i_b)}{dt} + E_A - E_B \quad (15)$$

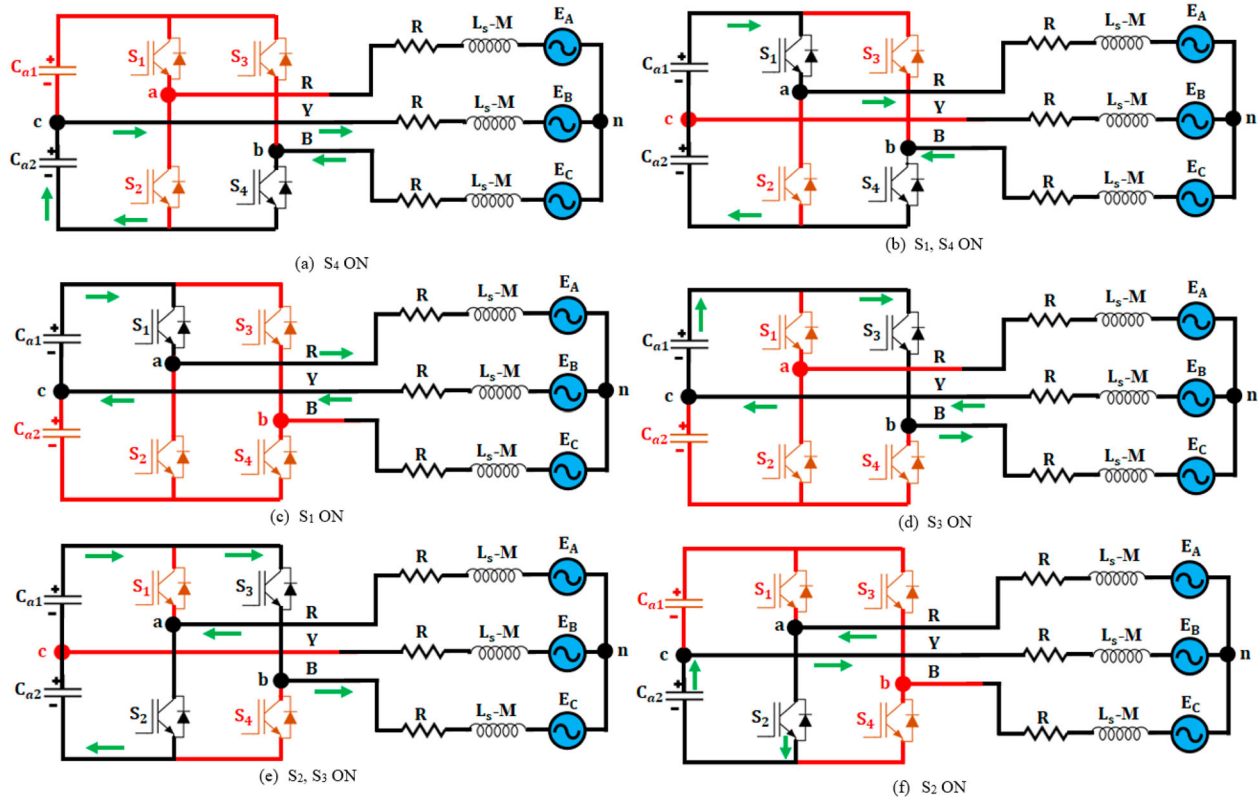


**Figure 8.** Four-switch VSI switching strategy.

$$V_{bc} = R(i_b - i_c) + L \frac{d(i_b - i_c)}{dt} + E_B - E_C \quad (16)$$

$$V_{ca} = R(i_c - i_a) + L \frac{d(i_c - i_a)}{dt} + E_C - E_A \quad (17)$$

The difference of the terminal voltages can be obtained as

$$V_{abbc} = R(i_a - 2i_b + i_c) + L \frac{d(i_a - 2i_b + i_c)}{dt} + E_A - 2E_B + E_C \quad (18)$$

Thus it is observed that the line voltage is a reversed depiction of back EMF waveform. It is perceived from Figure 9 that the back EMF is transferred from one polarity to other crossing zero. Hence, for revealing the

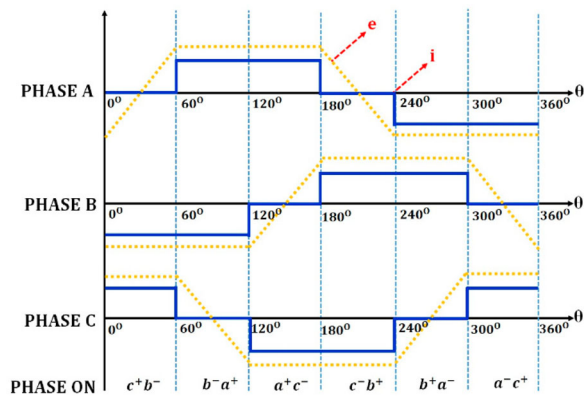


**Figure 9.** Back EMF and Phase current representation of BLDC motor.

zero crossing of phase B, operation  $V_{abbc}$  is enabled. Similarly  $V_{bcc a}$  has facilitated the zero detection crossing of phase C and  $V_{caab}$  has facilitated it for phase A. This back EMF is provided to the PI controller through the PWM generator.

### 3.5. Speed control of BLDC motor using Grey Wolf Optimization algorithm

When load is applied, there exists a change in motor speed, and in most of industrial applications, constant speed motors are preferred. In general, the closed-loop control is implemented by conventional PI controllers, which results in constant speed but there exist problems of maximum peak overshoot. To obtain better system responses, PI controllers are used widely in several industries. To overcome these overshoot problems, intelligence techniques like GA, PSO and GWO are utilized for optimized tuning of PI controllers. The GA shows slower convergence while the PSO has converged in the local optimum. Hence to attain better results, GWO algorithm is utilized, which prevents the falling in local optimum and the convergence is faster as that of wolf's behaviour.

#### GWO Algorithm

This is one of the population-based optimization algorithms, which has been used for tuning the PI controller. This algorithm is motivated by the common behaviour of grey wolves. The leadership order in the GWO algorithm is characterized as four clusters:

- Alpha ( $\alpha$ ) Dominant wolf, which makes decision can be either male or female.
- Beta ( $\beta$ ) Subordinate wolf, which aids alpha in decision making.
- Omega ( $\omega$ ) Lower ranking wolf.
- Delta ( $\delta$ ) Dominates omega and has to report alpha and beta.

The hunting behaviour and encircling can be modelled as follows:

$$\vec{D} = |\vec{C} \cdot \vec{G}_p(t) - \vec{G}(t)| \quad (19)$$

$$\vec{G}(t+1) = \vec{G}_p(t) - \vec{A} \cdot \vec{D} \quad (20)$$

where A, C, D are the coefficient vectors,  $t$  is the current in then-existing iterations,  $G_p$  and  $G$  are the position vector of prey and position vector of grey wolf respectively.

Coefficient vector A and C is measured by the following equations:

$$\vec{A} = 2\vec{a} \cdot \overrightarrow{rand_1} - \vec{a} \quad (21)$$

$$\vec{C} = 2 \cdot \overrightarrow{rand_2} \quad (22)$$

where “ $a$ ” reduces linearly from 2 to 0 during iterations  $rand_1$  and  $rand_2$ .

The number of duty ratios  $N_{ref}$  and  $N_{act}$  are measured through the sensors. Since the duty cycle (D) is determined as grey wolf, Equation (23) can be altered as,

$$D_i(k+1) = D_i(k) - A \cdot D \quad (23)$$

GWO fitness function is expressed as

$$P(D_i^k) > (D_i^{k-1}) \quad (24)$$

where power is denoted as  $P$ , number of present grey wolves is denoted as  $i$ , number of iterations is denoted as  $k$ . The objective function utilized here is integral absolute error (IAE).

$$IAE = \int_0^{\infty} |e(t)| dt \quad (25)$$

The GWO algorithm is as follows:

Step 1: Initialize vectors  $a$ , A and C.

Step 2: Initialize the number of iterations to zero ( $k = 0$ )

Step 3: Initialize the grey wolf pack size as 1 ( $i = 1$ )

Step 4: Measure  $N_{act}$  by the controller.

Step 5: Compare  $N_{ref}$  (3000 rpm) and  $N_{act}$  speeds for the converter.

Step 6: If  $N(i)$  is greater than  $N(i-1)$ , then update  $N_{max}$  where  $i = N(i)$ , else update  $N_{max}$ , where  $i = N(i-1)$

Step 7: Compare  $G_{max}$  with  $N_{max}$ , if  $G_{max}$  is greater update  $G_{max}$ . If  $G_{max}$  is less than  $N_{max}$ , check whether all agents are evaluated if yes update  $G_{max}$ , A, C by using

Equations (19), (20), (21), (22). If not moved to next wolf, go to step 4 and process till calculating the duty cycle.

Step 8: Repeat step 3 until convergence is met.

The population size is taken as 30 with 50 number of iterations. The foremost intent of the algorithm is to generate the duty cycle for the four-switch VSI to achieve speed control. By GWO algorithm, the reference signal is obtained and it is fed to the PWM generator (Hysteresis current control method), which generates the desired pulses that are then fed to the four-switch BLDC motor. By this control algorithm, speed in motor remains unchanged even when full load is applied.

#### 4. Result and discussion

The enactment of the proposed strategy is evaluated and the simulation is achieved by MATLAB. The outcomes are obtained and are discussed under no load, running and full load conditions. Speed, power, moment and EMF are considered for evaluating the performance of the system. As the PV output varies in accordance with the irradiance, it has a changing nature; it is not possible to feed such a variable output potential to load and so the output is nourished to the single-ended primary inductor converter, which is controlled with Fuzzy MPPT algorithm and provides a constant output voltage as shown in Figure 10. By implementing Fuzzy, the PV voltage and current are continuously checked and analogized with the previous values, from which the maximum value is chosen based on the rule base. The duty cycle of the SEPIC converter is directly generated by using Fuzzy MPPT and the converter's output voltage is 340 V. Based on the rules framed, the duty cycle is generated. Hence it is perceived that whenever there is a variation in the input, the output voltage remains unchanged. This output voltage is nourished to the BLDC motor through the four-switch set-up.

As the rotor of the BLDC motor has trapezoidal shape, the waveform of the current is non-sinusoidal and the shape is asymmetric as shown in Figure 11. In the starting (0–0.2 s) stage, it takes more current when the motor starts running and after that, the motor is run without any oscillations. In dynamic (0.2–0.5 s) and running (0.5–0.75 s) conditions, certain variations are there in current when the load is applied but the speed

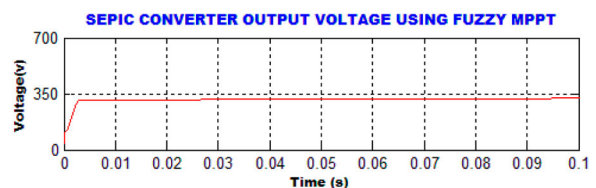


Figure 10. Output voltage of SEPIC converter with Fuzzy MPPT.

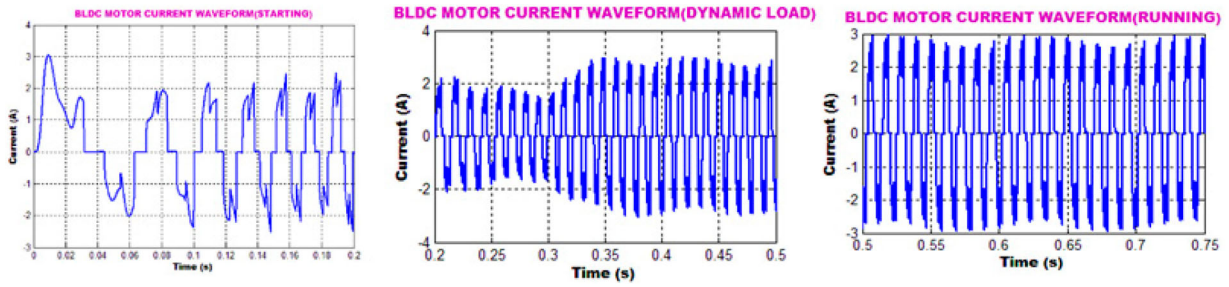


Figure 11. Current waveforms in starting, dynamic and running conditions.

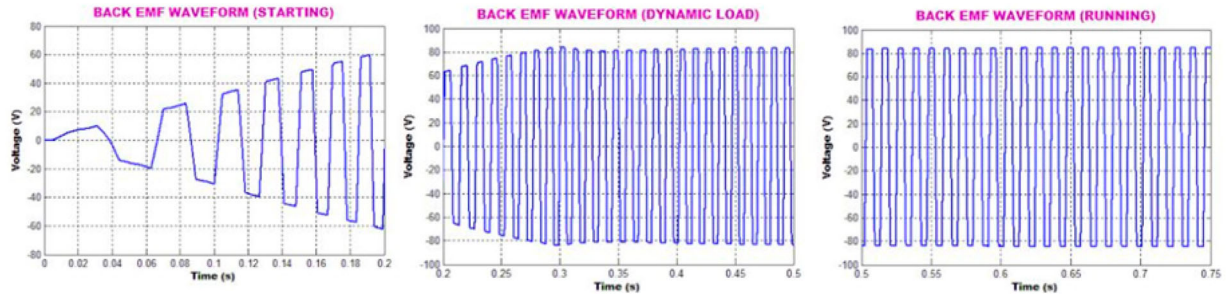


Figure 12. Back EMF waveforms in starting, dynamic and running conditions.

in the motor gets unaffected. As the nature of back EMF in brushless DC motor is trapezoidal, the waveforms are obtained as shown in Figure 12.

As no load is applied in the starting condition, back EMF is very less but when the load is applied gradually, the back EMF gets increased. During the dynamic and the running conditions, its value ranges from +80 V to -80 V. Torque waveform in BLDC motor is revealed

in Figure 13. As motor draws more current during the starting stage, the starting torque is also high but when the load is applied, there exists a variation in the torque yet it is noted that the speed of the motor is not affected.

For the speed control of the BLDC motor, GWO-PI is utilized which is designed based on the behaviour of grey wolves; speed waveform of the BLDC motor is highlighted in Figure 14; when load is applied (at 0.3 s),

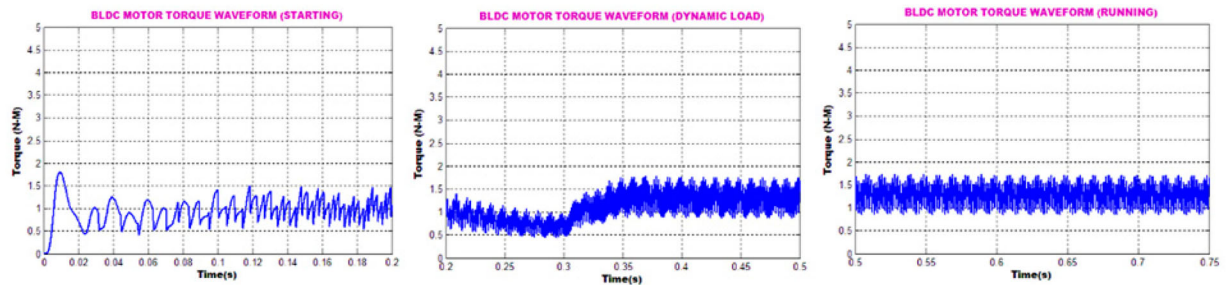


Figure 13. Torque waveforms in starting, dynamic and running conditions.

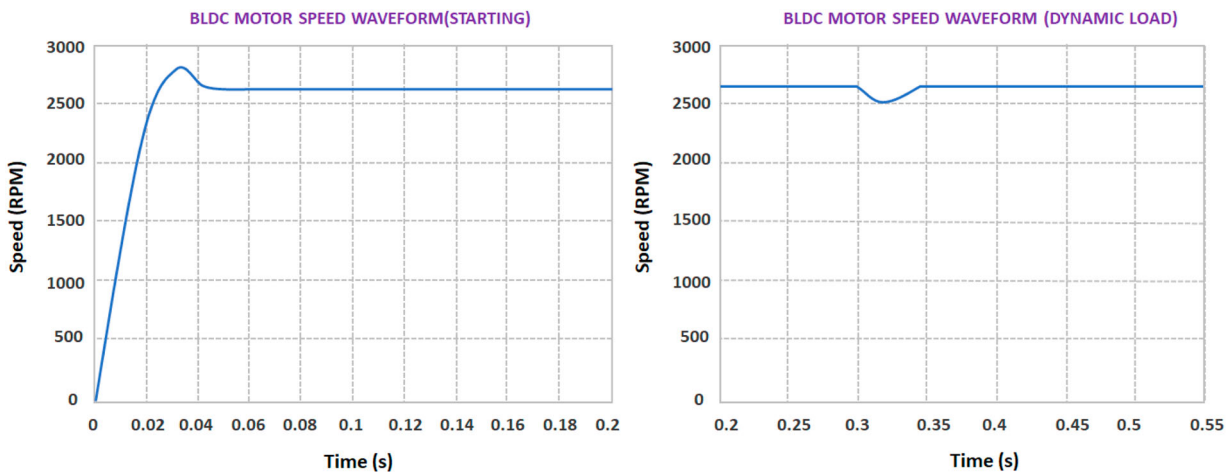


Figure 14. Speed waveform.



Figure 15. Hardware setup

the GWO algorithm stands good with a settling time of 0.0375 s. As a closed-loop control with optimization technique is implemented, the motor speed settles faster.

**Hardware implementation**

The proposed strategy involves the analysis of solar fed four-switch Brushless DC motor drive. To achieve the desired speed, closed-loop control has been instigated with PI controller, which is tuned through GWO algorithm. The results are perceived through simulation and it is clear that the motor’s speed is unaffected with any change in the load even at full load condition. This can also be implemented in hardware (Figure 15) by using the FPGA Spartan 6E controller.

It is perceived that the resultant output voltage of PV remains the same for any variation in the climate. It is clearly depicted in Figure 16(a) and (b). The MPPT controller takes the values of voltage and current, from which the required input for the fuzzification is computed and the rules are selected. Based on the decision of the rules, the values are defuzzified and the corresponding duty ratio is given to the converter. The output obtained from single-ended primary inductor converter is depicted in Figure 17. It is noticed that the ripples are highly minimized by the application of this converter. The current and speed waveform of BLDC motor is observed in Figure 18(a) and (b). Hence in hardware implementation, it has been observed that the

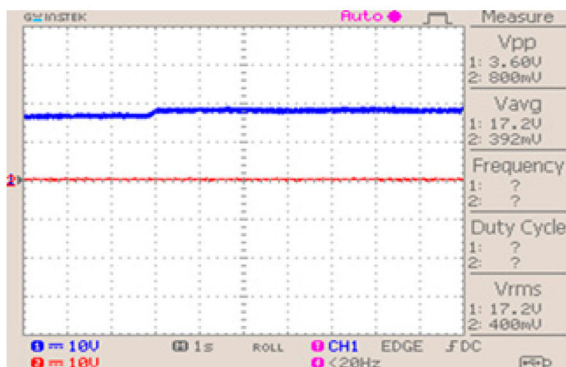


Figure 16. (a) PV irradiation and (b) PV voltage.

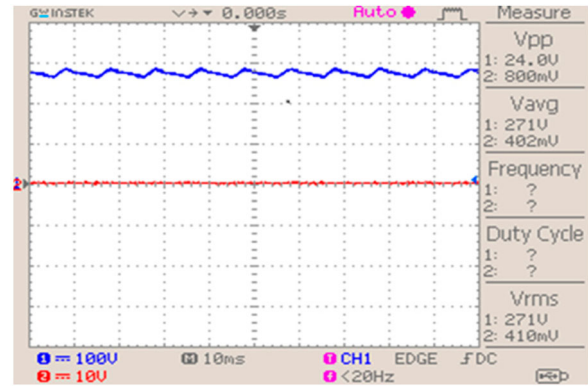


Figure 17. Output of SEPIC converter.

Table 3. Comparison of six-switch and four-switch strategies.

	Six-switch strategy	Four-switch strategy
No. of switches	6	4
Switching losses	High	Less
Cost	High	Less
Control algorithms	Complex	Simple

speed of the motor settles at 2750 rpm with a settling time of 0.07 s.

Comparison of Brushless DC motor speed is revealed in Figure 19. The hardware results are compared by applying various control algorithms and it is perceived that the GWO algorithm shows less variations. When load is applied, it is perceived that the speed decreases and by the GWO algorithm, the waveform settles at 0.07 sec even after the load is applied.

Figure 20(a) and (b) shows the outputs of Brushless DC motor driven by six-switch strategy and four-switch strategy respectively. And it is perceived that the response of four-switch strategy takes more time to settle when compared to six-switch strategy.

Table 3 gives a detailed comparison of the four-switch and six-switch strategies. As the number of switches used is less, the cost, size and complexity associated with switches are minimized.

The switching loss relies on the switching frequency and the formula is given as

$$W_{\text{switch}} = \frac{V_{\text{min}} I_{\text{max}}}{6} (T_{\text{ON}} + T_{\text{OFF}}) f_{\text{sw}} \quad (26)$$

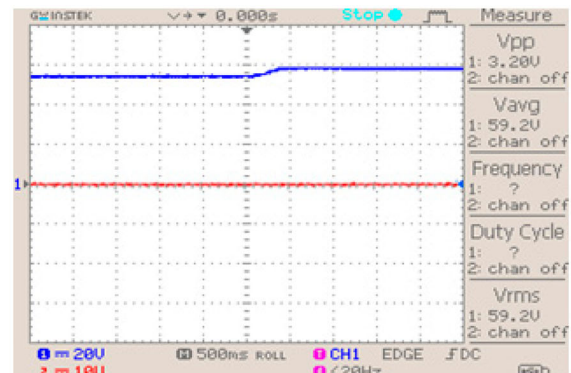




Figure 18. (a) Current waveform of BLDC motor and (b) speed waveform of BLDC motor.

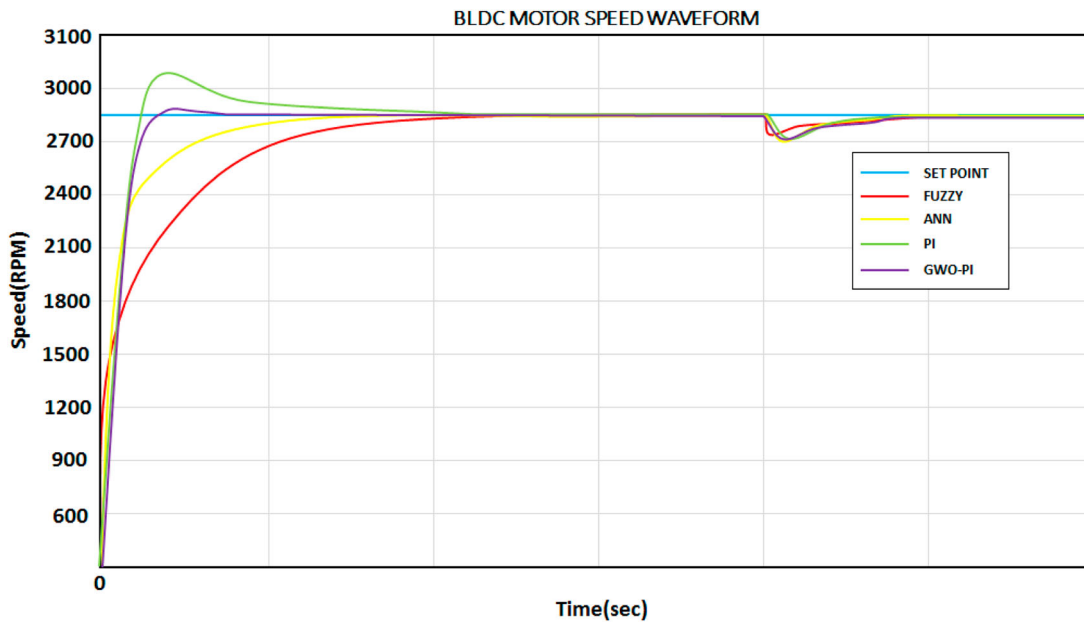


Figure 19. Comparison of speed.

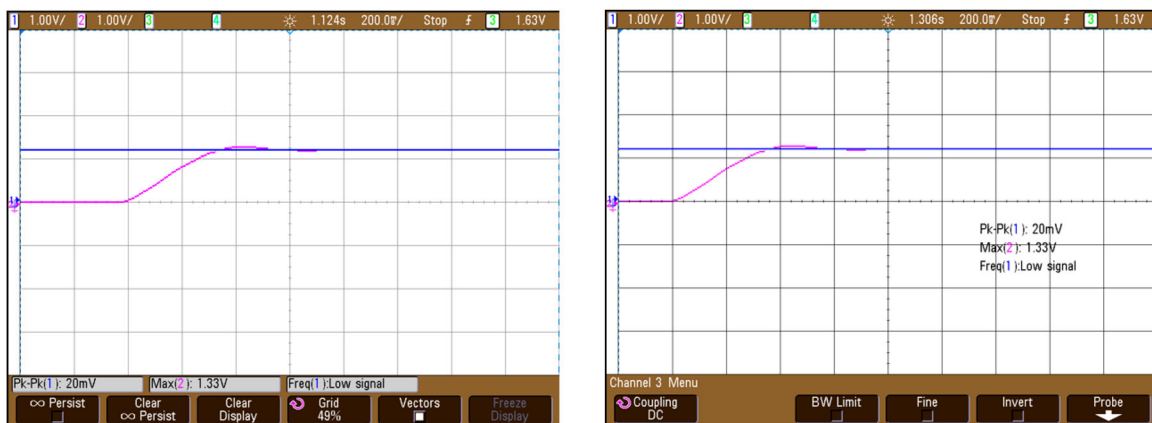


Figure 20. Output of BLDC drive with (a) six-switch strategy and (b) four-switch strategy.

The ON and OFF time are taken as  $1.2\mu s$  and  $1.5\mu s$  with switching frequency ( $f_{sw}$ ) as 10 kHz; the minimum voltage ( $V_{min}$ ) and the maximum current ( $I_{max}$ ) are taken as 100 V and 3A respectively. By substituting these values, the switching losses for a single switch are obtained as 1.35 W.

The switching losses for six switches are obtained as  $6 \times 1.35 = 8.1 W$ , whereas the switching losses for four switches is obtained as  $4 \times 1.35 = 5.4 W$ .

By incorporating the Grey Wolf Optimization technique, four-switch VSI is more effective. Currently, the four-switch VSI is applicable for all BLDC drives

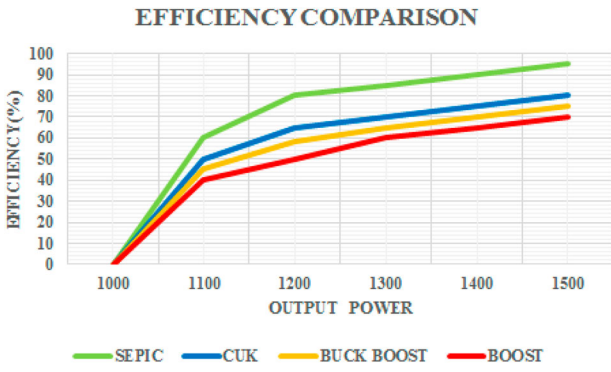


Figure 21. Comparison of efficiency.

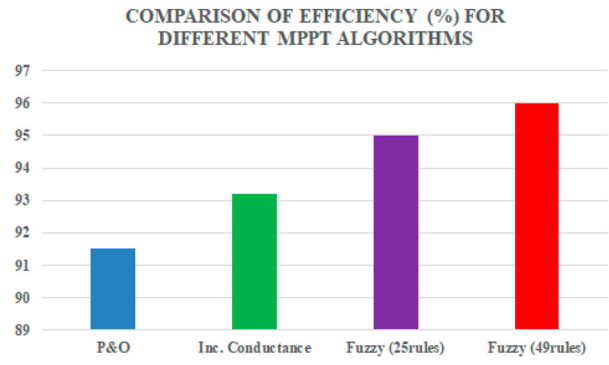


Figure 23. Comparison of Efficiency for different MPPT algorithms.

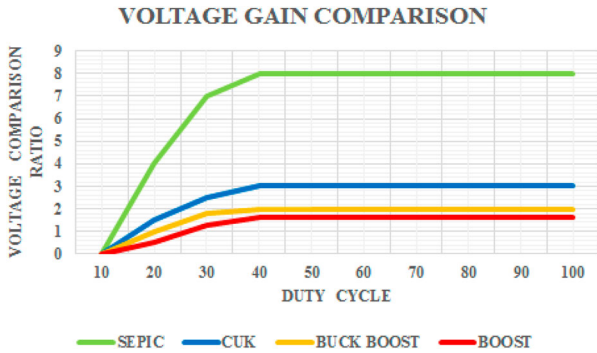


Figure 22. Comparison of voltage gain.

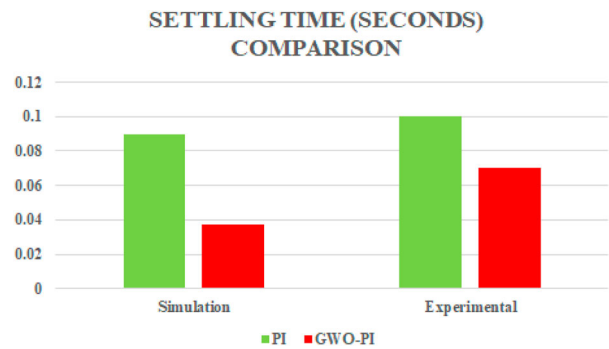


Figure 24. Settling Time Comparison with PI and GWO-PI.

Table 4. Voltage-gain and efficiency comparison.

Converter	Voltage gain	Efficiency
Boost	1:1.5	70%
Buck-Boost	1:2	75%
Cuk	1:3	80%
SEPIC	1:8	96%

because of its compact size, reduction in switching driver circuits and cost.

Figure 21 has depicted the comparison of the efficiency of converters such as SEPIC, CUK, BUCK BOOST, BOOST for different output power. This shows that a maximum efficiency of 96% can be attained by SEPIC while other topologies result in lesser efficiency.

Figure 22 shows the voltage gain of various converters like SEPIC, CUK, BUCK BOOST and BOOST. It is perceived that the voltage gain can be measured by varying the duty cycle and the gain is increasing from 0 to 8 in the case of SEPIC converter while the gain of other converters is lesser than the SEPIC converter. The values of the efficiency and the voltage-gain are given in Table 4.

The performance of SEPIC converter employing Fuzzy-based MPPT algorithm with 49 rules is compared with P&O, Incremental conductance and Fuzzy MPPT with 25 rules and it is revealed that the Fuzzy MPPT with 49 rule-base is superior to other algorithms with an efficiency of 96% (Figure 23).

The performance of the GWO-PI for motor speed control is analogized with that of the PI controller and the observations are made as in Figure 24. By using

GWO-PI, the settling time is observed as 0.0375 and 0.07 s for the simulation and experimental observation respectively; whereas with PI controller, the settling time is observed as 0.09 and 0.1 s for simulation and experimental observation respectively.

### 5. Conclusion

The analysis of sensorless speed control in four-switch BLDC motor drive fed by PV system is done in this paper. The output potential of single-ended primary inductor converter is retained by means of Fuzzy Logic MPPT algorithm. By using SEPIC converter, the ripples are greatly minimized. The efficiency of SEPIC converter is observed as 96%, from the simulations. SEPIC converter exhibits a high voltage gain of 1:8. The reliability of the proposed strategy is evaluated under no load condition, running condition and dynamic load condition of brushless DC motor. The effectiveness of the proposed strategy is analysed through simulation and real-time tactics. The behaviour of the system is analysed in the absence of sensors, which is cost effective. The cost and size are minimized by the use of four-switch VSI strategy. An effective speed control is achieved by PI controller, which is tuned by using the GWO algorithm even under full load condition. A detailed analysis of proposed strategy and existing strategy is compared and simulation results are validated.

## Disclosure statement

No potential conflict of interest was reported by the author(s).

## References

- [1] Shen J, Qin X, Wang Y. High-speed permanent magnet electrical machines — applications, key issues and challenges. *CES Trans Electr Mach Syst.* 2018;2(1):23–33.
- [2] de Almeida PM, Valle RL, Barbosa PG, et al. Robust control of a variable-speed BLDC motor drive. *IEEE J Emerg Sel Top Ind Electron.* 2021;2(1):32–41.
- [3] Valle RL, De Almeida PM, Fogli GA, et al. Simple and effective digital control of a variable-speed low inductance BLDC motor drive. *IEEE Access.* 2020;8:13240–13250.
- [4] Shanmugasundram R, Zakariah KM, Yadaiah N. Implementation and performance analysis of digital controllers for brushless DC motor drives. *IEEE Trans Mechatron.* 2014;19(1):213–224.
- [5] Trivedi MS, Keshri RK. Evaluation of predictive current control techniques for PM BLDC motor in stationary plane. *IEEE Access.* 2020;8:46217–46228.
- [6] Gruebler H, Leitner S, Muetze A, et al. Improved switching strategy for a single-phase brushless direct current Fan drive and its impact on efficiency. *IEEE Trans Ind Appl.* 2018;54(6):6050–6059.
- [7] Kolano K. Improved sensor control method for BLDC motors. *IEEE Access.* 2019;7:186158–186166.
- [8] Chen S, Liu G, Zhu L. Sensorless control strategy of a 315 kW high-speed BLDC motor based on a speed-independent flux linkage function. *IEEE Trans Ind Electron.* 2017;64(11):8607–8617.
- [9] Chen X, Liu G. Sensorless optimal commutation steady speed control method for a nonideal back-EMF BLDC motor drive system including buck converter. *IEEE Trans Ind Electron.* 2020;67(7):6147–6157.
- [10] Lee Y, Kim J. Analysis of the three-phase inverter power efficiency of a BLDC motor drive using conventional six-step and inverted pulsewidth modulation driving schemes. *Can J Electr Comput Eng.* 2019;42(1):34–40.
- [11] Tian B, An Q-T, Molinas M. High-frequency injection-based sensorless control for a general five-phase BLDC motor incorporating system delay and phase resistance. *IEEE Access.* 2019;7:162862–162873.
- [12] Sashidhar S, Guru Prasad Reddy V, Fernandes BG. A single-stage sensorless control of a PV-based bore-well submersible BLDC motor. *IEEE J Emerg Sel Top Power Electron.* 2019;7(2):1173–1180.
- [13] Kumar R, Singh B. Single stage solar PV fed brushless DC motor driven water pump. *IEEE J Emerg Sel Top Power Electron.* 2017;5(3):1377–1385.
- [14] Kumar R, Singh B. Solar PV powered-sensorless BLDC motor driven water pump. *IET Renew Power Gener.* 2019;13(3):389–398.
- [15] Kumar R, Singh B. Grid interactive solar PV-based water pumping using BLDC motor drive. *IEEE Trans Ind Appl.* 2019;55(5):5153–5165.
- [16] Kumar A, Sensarma P. A four-switch single-stage single-phase buck-boost inverter. *IEEE Trans Power Electron.* 2017;32(7):5282–5292.
- [17] Aghdam FH, Abapour M. Reliability and cost analysis of multistage boost converters connected to PV panels. *IEEE J Photovoltaics.* 2016;6(4):981–989.
- [18] de Morais J, de Morais J, Gules R. Photovoltaic AC module based on a Cuk converter with a switched-inductor structure. *IEEE Trans Ind Electron.* 2019;66(5):3881–3890.
- [19] Bollipo R, Mikkili S, Bonthagorla PK. Critical review on PV MPPT techniques: classical, intelligent and optimisation. *IET Renew Power Gener.* 2020;14(9):1433–1452.
- [20] Bollipo RB, Mikkili S, Bonthagorla PK. Hybrid, optimal, intelligent and classical PV MPPT techniques: a review. *CSEE J Power Energy Syst.* 2021;7(1):9–33.